ACS OMEGA

http://pubs.acs.org/journal/acsodf

Article

Influence of the ZnCrAl Oxide Composition on the Formation of Hydrocarbons from Syngas

Tobias Kull, Thomas Wiesmann, Andrea Wilmsen, Maximilian Purcel, Martin Muhler, Heiko Lohmann, Barbara Zeidler-Fandrich, and Ulf-Peter Apfel*

Cite This: *ACS Omega* 2022, 7, 42994−43005

Read Online

ACCESS | Metrics & More | Article Recommendations | Supporting Information

ABSTRACT: The conversion of syngas into value-added hydrocarbons gains increasing attention due to its potential to produce sustainable platform chemicals from simple starting materials. Along this line, the "OX-ZEO" process that combines a methanol synthesis catalyst with a zeolite, capable of catalyzing the methanol-to-hydrocarbon reaction, was found to be a suitable alternative to the classical Fischer−Tropsch synthesis. Hitherto, understanding the mechanism of the OX-ZEO process and simultaneously optimizing the CO conversion and the selectivity toward a specific hydrocarbon remains challenging. Herein, we present a comparison of a variety of ZnCrAl oxides with different metal ratios combined with a H-ZSM-5 zeolite for the conversion of syngas to hydrocarbons. The effect of aluminum on the catalytic activity was investigated for ZnCrAl oxides with a Zn/Cr ratio of 4:1, 1:1, and 1:2. The product distribution and CO conversion were found to be strongly influenced by the Zn/Cr/Al ratio. Although a ratio of Zn/Cr of 1:2 was best to produce lower olefins and aromatics, with aromatic selectivities of up to 37%, catalysts with a 4:1 ratio revealed high paraffin selectivity up to 52%. Notably, a distinct effect of aluminum in the oxide lattice on the catalytic activity and product selectivity was observed, as a higher Al content leads to a lower CO conversion and a changed product spectrum. We provide additional understanding of the influence of different compositions of ZnCrAl oxides on their surface properties and the catalytic activity in the OX-ZEO process. Furthermore, the variation of the zeolite component supports the important role of the channel topology of the porous support material for the hydrocarbon production. In addition, variation of the gas hourly space velocity showed a correlation of contact time, CO conversion, and hydrocarbon selectivity. At a gas hourly space velocity of 4200 mL/g_{cat} h, CO conversion as high as 44% along with a CO_2 selectivity of 42% and a lower paraffin (C_2^0−C_4^0) selectivity of 41% was observed.

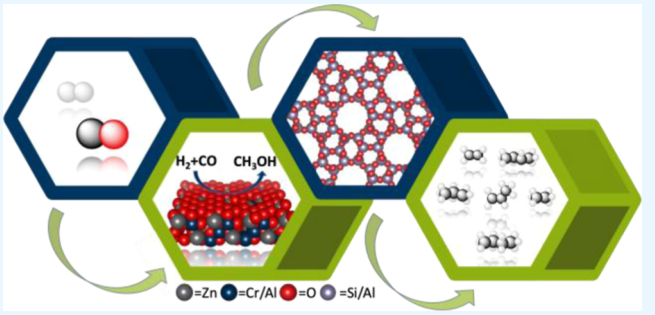

INTRODUCTION

Syngas has a long-standing history in the chemical industry as a versatile carbon source and recently experienced increasing interest due to its potential to act as a sustainable feedstock.[1−4] This mixture of CO and H_2 can be derived from a variety of resources including biogas, natural gas, and coal.[5,6] In addition, power-to-syngas concepts likewise aim for the electrochemical reduction of CO_2 to CO along with the production of H_2.[6−9] This offers a sustainable path toward syngas and subsequently value-added hydrocarbons, such as lower olefins or aromatics via Fischer−Tropsch synthesis (FTS) and thus enables a more sustainable chemical industry via non-fossil routes. Yet, the FTS selectivity toward lower olefins is limited due to aliphatic chain growth described by the Anderson−Schulz−Flory distribution.[10−12] Therefore, alternative processes following different reaction mechanisms and thereby bypassing the aliphatic chain growth are of great need.

In 1978, Chang et al. developed a process that combines a methanol synthesis catalyst with acidic zeolites used for the conversion of methanol to hydrocarbons and enabled the syngas conversion into hydrocarbons with high selectivity.[13] Recently, this process gained increasing interest initialized by the findings of Jiao et al. who combined metal oxides with acidic zeolites and referred to this reaction as the "OX-ZEO process".[14,15] By now, various combinations of metal oxides (e.g., MnO, Mo−ZrO_2, $ZnGa_2O_4$, and In_2O_3) and zeolites (SAPO-34, H-MOR, SSZ-13, and AlPO-18) were investigated toward their capability of producing specific hydrocarbons with high selectivities.[15−22] Yet, a key research question that is still not unequivocally resolved is the nature of the intermediate species that is produced by the oxide and then transferred to

Received: August 15, 2022
Accepted: October 13, 2022
Published: November 16, 2022

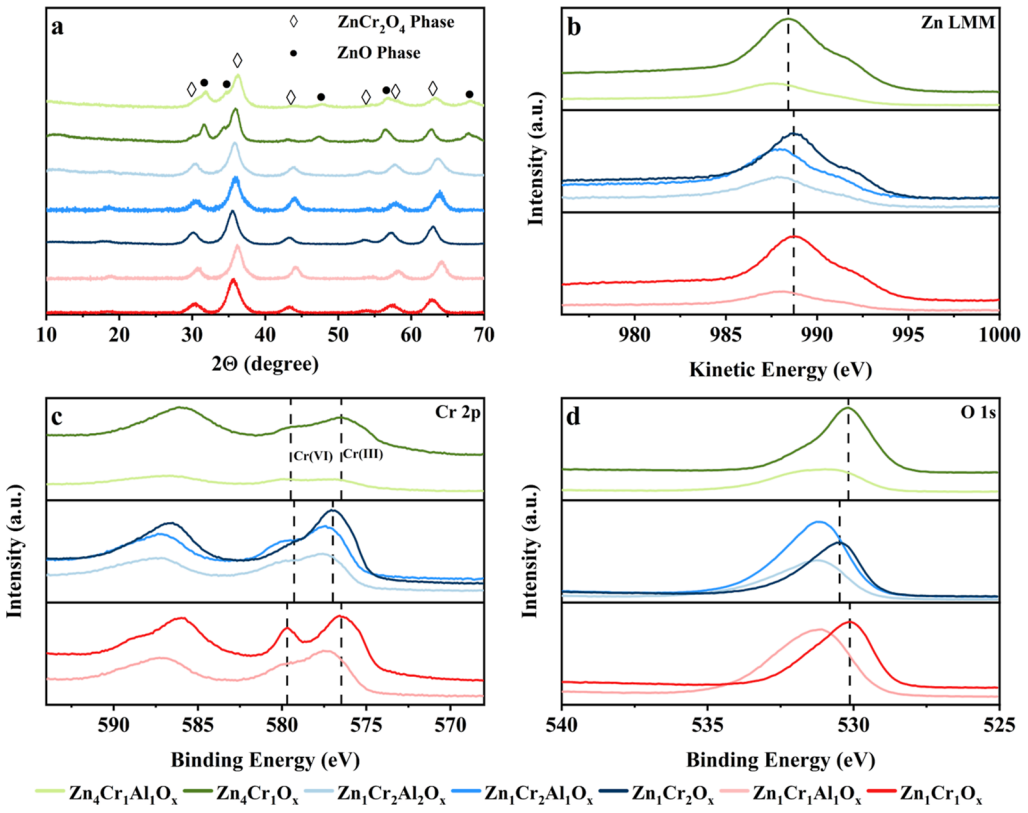

Figure 1. (a) PXRD patterns of herein prepared oxides; (b) Auger Zn $L_3M_{4.5}M_{4.5}$ peaks; and XPS (c) Cr 2p and (d) O 1s spectra of the ZnCrAl oxides with varying metal ratios.

the zeolite.[14,21] Along this line, a ketene intermediate was observed over a catalyst composed of $ZnCrO_x$ and SAPO-34 by highly sensitive synchrotron-based vacuum ultraviolet photoionization mass spectrometry (SVUV-PIMS).[14] Likewise, methanol was excluded as a potential reaction intermediate because the pure zeolite fed with methanol was quickly deactivated and showed poor long-term stability, thus contradicting the experimental findings of the OX-ZEO process. Furthermore, the absence of formate as an intermediate was reported investigating Mn−Ga oxide and SAPO-34 by in situ diffuse reflectance infrared Fourier transform spectroscopy (DRIFTS).[23] Herein, the observed vibration bands after the adsorption of pure CO and syngas on the surface of the bifunctional catalyst were assigned to O−C−O stretching. Only upon elongated exposure of the catalyst to syngas, a weak C−H stretching band was observed indicating the presence of surface carbonate species rather than a formate intermediate. Hence, the authors deduced that ketene acts as the key reaction intermediate in this process. In contrast, Liu et al. observed formate species caused by CO adsorption on Zn-doped ZrO_2 nanoparticles which are likely converted to methoxide species and eventually to methanol after switching the gas stream from CO to CO/H_2.[21] This assumption was further supported by the finding that the zeolite alone fed with methanol and H_2 shows a similar conversion of the reagent gas as the composite catalyst. Methanol conversion over SSZ-13 increased gradually with the density of Brønsted acid sites up to 97%. An identical trend was observed for the CO conversion over the combination of Zn-doped ZrO_2 and SSZ-13. Furthermore, the selectivity for lower olefins ($C_2^=-C_4^=$) for both, the single zeolite material and the composite catalyst decreased with increasing Brønsted acid sites, whereas the lower paraffin ($C_2^0-C_4^0$) selectivity increased. These similarities between the conversion of methanol over the sole zeolite catalyst and the CO conversion over the bifunctional catalyst indicate a reaction mechanism that proceeds via the formation of methanol over the oxide and the conversion of methanol to hydrocarbons over the zeolite and is in stark contrast to the results showing ketene as a key intermediate.

An additional persisting issue in the OX-ZEO process that remains to be solved is the combination of high selectivity toward a specific hydrocarbon product and high CO conversion, along with low CO_2 selectivity. Typically, CO_2 is produced via the water gas shift reaction as major byproduct by the metal oxide.[24−27] Notably, Huang et al. reached a $C_2^=-C_4^=$ selectivity of up to 88% among the produced hydrocarbons with a CO conversion of 18% over $ZnCrO_x$ and nanosized sheet-like SAPO-34.[28] However, the CO_2 selectivity was still as high as 50%. A significantly lower CO_2 selectivity of 5.7% was observed for $Zn_{0.3}Ce_{1.0}Zr_{1.0}O_4$/SAPO-34 accompanied by high $C_2^=-C_4^=$ selectivities of up to 83%.[29] Unfortunately, the CO conversion was found to be as low as 6.4%. These examples show that although high hydrocarbon selectivity and CO conversion can be reached, both are opposite to the CO_2 selectivity, which is preferably low.

Obviously, further studies that clarify the reaction mechanism and offer new insights into optimization possibilities for the OX-ZEO process are needed. One important aspect that could lead to an enhanced understanding is to identify the influence of the metal oxide components on the product distribution. Notably, many OX-ZEO catalysts reported in the literature consist of ZnCr oxides as one catalyst component.[17,25,30−34] For example, Arslan et al. obtained a

https://doi.org/10.1021/acsomega.2c05225
ACS Omega 2022, 7, 42994−43005

selectivity of 70% for tetramethylbenzene together with a CO conversion of 37% and a CO_2 selectivity of about 50% using a $ZnCr_2O_4$ spinel oxide jointly with H-ZSM-5 in a stream of H_2 deficient syngas.[35] Likewise, a combination of SAPO-34 with a series of ZnCr oxides with varying Zn/Cr ratios ranging from 4:1 to 1:3 revealed a significant effect of the metal oxide composition on the OX-ZEO process.[36] The oxide with a Zn/Cr ratio of 1:1 was found to be best suited for the conversion of syngas to lower olefins, which was ascribed to optimal $ZnO-ZnCr_2O_4$ interfaces present in this oxide. Furthermore, ZnAl oxides were tested toward their catalytic activity in the OX-ZEO process.[24,37,38] For example, $ZnAl_2O_4$ spinel oxide in combination with SAPO-34 led to a $C_2^=-C_4^=$ selectivity of 80%, a CO conversion of 24%, and a CO_2 selectivity of 44%.[17] Next to binary materials, ternary ZnCrAl oxides were reported.[14,39−41] Along this line, the ternary oxide Zn_3CrAlO_x in combination with H-ZSM-5 produced 74% aromatics and 47% CO_2 at a CO conversion rate of 16%.[42] Although the influence of different Zn/Cr ratios in the binary oxides has been widely studied, the effect of aluminum incorporated into the binary oxides remains unclear. Although aluminum in the form of α-Al_2O_3 is often used as dilutant or support material due to its inert characteristics, incorporation of Al atoms into the crystal lattice of the metal oxide is expected to significantly influence the catalyst structure and its catalytic properties. Hence, we investigated the synthesis of ZnCrAl oxides with varying metal ratios along with catalytic tests utilizing combinations of these oxides and commercial H-ZSM-5 zeolite. The effect of the direct incorporation of aluminum during the synthesis of ZnCr oxides was investigated for materials with Zn/Cr ratios of 4:1, 1:1, and 1:2 to cover oxides with excess Zn, an equimolar ratio, and the stoichiometric ratio for spinel compounds. Furthermore, the effect of different zeolites (FAU-15, H-ZSM-5, and Fe-BEA-35) combined with the ZnCrAl oxides along with the variation of the space velocity were studied.

RESULTS AND DISCUSSION

Catalyst Characterization. The oxide component of the OX-ZEO catalyst and its structural properties play a crucial role in the conversion of syngas to hydrocarbons. Hence, various ZnCrAl oxides of the general composition $Zn_aCr_bAl_cO_x$ (a = 1, 4; b = 1, 2; for b = 1: c = 0, 1; for b = 2: c = 0, 1, 2) were prepared via the co-precipitation method reported by Jiao et al.[14] and characterized by powder X-ray diffraction (PXRD), XPS, and N_2 sorption techniques.

A comparison of the PXRD patterns of the synthesized oxides is given in Figure 1a. Notably, a pure cubic spinel phase can be observed for $Zn_1Cr_1Al_cO_x$ and $Zn_1Cr_2Al_cO_x$ oxides. In contrast, for materials comprising an excess of Zn ($Zn_4Cr_1Al_cO_x$), a mixture of the cubic spinel phase together with a ZnO phase is present. These observations are in line with theoretical calculations conducted by Ma et al. who found that ZnCr oxides crystallize in a spinel lattice for Zn/Cr ratios of up to 1:1 and show a distinct ZnO phase for ratios larger than 1:1.[43] Markedly, the aluminum content of the materials studied here has no obvious effect on the formed crystal phase. Incorporation of Al into the synthesis mixture of the ZnCrAl oxides did not lead to any additional reflections in the PXRD patterns and neither reflections for the spinel $ZnAl_2O_4$ nor Al_2O_3 were found. This suggests the successful integration of Al into the spinel crystal lattice. To better understand the electronic environment of the metal ions within the oxides, X-ray photoelectron spectroscopy (XPS) was conducted. The XPS analysis shows a kinetic energy of 988.7 eV (Figure 1b) for the Zn $L_3M_{4.5}M_{4.5}$ Auger peak of $Zn_1Cr_2O_x$. Incorporation of Al into the spinel lattice leads to a decrease in the kinetic energy to 987.9 eV for $Zn_1Cr_2Al_cO_x$, which highlights the changed electron density around the Zn atoms due to Al incorporation. Further increase of the Al content in $Zn_1Cr_2Al_2O_x$, however, does not further affect the kinetic energy. Obviously, lowering the Cr content has no significant influence on the electronic properties of Zn as is visible by a kinetic energy of 988.7 eV for $Zn_1Cr_1O_x$. Yet, also for the $Zn_1Cr_1Al_cO_x$ oxides, incorporation of Al again leads to a decrease in kinetic energy as is evidenced by the lowered Zn $L_3M_{4.5}M_{4.5}$ energy of 987.8 eV for $Zn_1Cr_1Al_1O_x$. Similar kinetic energies for the Zn $L_3M_{4.5}M_{4.5}$ Auger peaks of $Zn_1Cr_2Al_cO_x$ and $Zn_1Cr_1Al_cO_x$ oxides further support the structural similarity suggested by the PXRD patterns.

For completeness, an excess of Zn in the oxide material has likewise no significant effect on the electronic properties of Zn, as the Zn $L_3M_{4.5}M_{4.5}$ Auger peak for $Zn_4Cr_1O_x$ is detected at a kinetic energy of 988.3 eV. Again, incorporation of Al leads to a decrease in kinetic energy to 978.5 eV for $Zn_4Cr_1Al_1O_x$. The trends that can be observed for the Cr 2p and O 1s spectra (Figure 1c,d) are similar to the trends for the Zn $L_3M_{4.5}M_{4.5}$ Auger peaks. However, it should be noted that in the Cr 2p XPS spectra two Cr species are visible. At a binding energy of around 576.5 eV, the Cr(III) species in the spinel $ZnCr_2O_4$ is detected, and at around 579.5 eV, a Cr(VI) species can be observed. The amount of the chromate species on the oxide surface increases with the Al content of the material (see Figure S1 and Table S1).

In summary, XPS analysis reveals a significant effect of the incorporation of Al on the electronic properties of the ZnCrAl oxide surface.

To gain deeper insights into the surface texture of the oxides, scanning electron microscopy (SEM) images were recorded and energy-dispersive X-ray spectroscopy (EDX) mapping was performed to obtain information about the element distribution on the surface (Figure S2). As can be seen from the EDX analysis, the distribution of Zn, Cr, and Al on the surface is homogeneous which suggests a successful incorporation of Al into the ZnCr oxides. An even deeper insight into the particle morphology was obtained by TEM measurements (Figure 2) that show agglomerates of sphere-like nanoparticles with a diameter of roughly up to 10 nm independent of the elemental composition. Analysis of the lattice spacing in the different oxides revealed lattice spacings of $ZnCr_2O_4$ and ZnO, but no lattice fringes for $ZnAl_2O_4$ or Al_2O_3 were found (Figure S3) which is consistent with the PXRD analysis.

Subsequently, we investigated the surface size and pore properties by multilayer N_2 physisorption measurements (BET) (Table 1). Clearly, the pure spinel phase present in $Zn_1Cr_2Al_cO_x$ and $Zn_1Cr_1Al_cO_x$ provides a higher surface area in contrast to the mixed phases composed of spinel $ZnCr_2O_4$ and ZnO (e.g., in $Zn_4Cr_1Al_cO_x$). The lowest surface area was observed for $Zn_4Cr_1O_x$ with 103 m^2/g, which increased to 125 m^2/g with incorporation of Al to form $Zn_4Cr_1Al_1O_x$. Generally, incorporation of Al leads to an increase of the surface area of the oxides. For example, the surface area of $Zn_1Cr_2O_x$ (137 m^2/g) increased to 174 m^2/g upon incorporation of one equivalent of Al and further increases to 220 m^2/g for $Zn_1Cr_2Al_2O_x$ containing two Al equivalents. It is likewise worth mentioning that this trend is much more pronounced for the

https://doi.org/10.1021/acsomega.2c05225
ACS Omega 2022, 7, 42994−43005

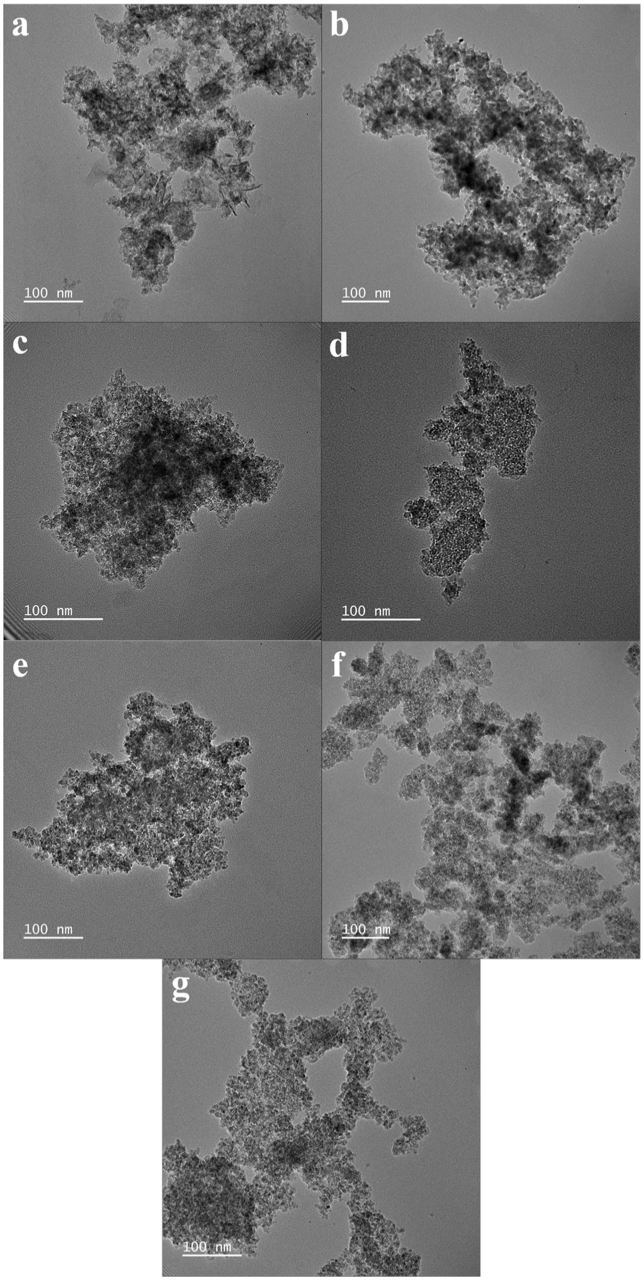

Figure 2. High-resolution transmission electron microscopy (HR-TEM) images of (a) $Zn_4Cr_1Al_1O_x$, (b) $Zn_4Cr_1O_x$, (c) $Zn_1Cr_2Al_2O_x$, (d) $Zn_1Cr_2Al_1O_x$, (e) $Zn_1Cr_2O_x$, (f) $Zn_1Cr_1Al_1O_x$, and (g) $Zn_1Cr_1O_x$.

Table 1. N_2 Physisorption Properties of the ZnCrAl Oxides

oxide	BET surface area (m^2/g)	total pore volume[a] (cm^3/g)
$Zn_4Cr_1Al_1O_x$	125	0.34
$Zn_4Cr_1O_x$	103	0.53
$Zn_1Cr_2Al_2O_x$	220	0.55
$Zn_1Cr_2Al_1O_x$	174	0.50
$Zn_1Cr_2O_x$	137	0.36
$Zn_1Cr_1Al_1O_x$	255	0.95
$Zn_1Cr_1O_x$	110	0.20

[a]The total pore volume was determined at $p/p_0 = 0.95$.

$Zn_1Cr_1Al_cO_x$ oxide series as $Zn_1Cr_1Al_1O_x$ shows a more than doubled surface area with 255 m^2/g compared to $Zn_1Cr_1O_x$ (110 m^2/g).

Along this line, the total pore volumes of the $Zn_1Cr_2Al_cO_x$ and $Zn_1Cr_1Al_cO_x$ oxide series show a similar trend as for both series an increase of the volume can be observed with increasing Al content. Although for $Zn_1Cr_2O_x$ the total pore volume was found to be 0.36 cm^3/g, it increases with each equivalent of Al up to 0.55 cm^3/g for $Zn_1Cr_2Al_2O_x$. Interestingly, the total pore volume of $Zn_1Cr_1O_x$ is with 0.20 cm^3/g very small compared to the other materials but increases strongly upon Al incorporation to yield the highest volume of all measured oxides with 0.95 cm^3/g for $Zn_1Cr_1Al_1O_x$.

For a complete understanding of the structure−activity relationship of the two-component OX-ZEO catalyst, next to the structural properties of the oxide, structural and acidic properties of the zeolite component are likewise crucial. The oxide component was mixed with commercial H-ZSM-5, FAU-15, or Fe-BEA-35 zeolites, respectively, to form the two-component catalyst. Although available from the vendors, textural properties of the zeolite components were obtained by N_2 physisorption measurements, which are listed in Table 2. The highest values are found for FAU-15 with a surface area, a pore volume, and a median pore width of 751 cm^2/g, 0.25 cm^3/g, and 1.2 nm, respectively, followed by Fe-BEA-35. The smallest values were observed for H-ZSM-5 with a surface area of 468 cm^2/g, a pore volume of 0.08 cm^3/g, and a median pore width of 0.88 nm. Notably, in the conversion of methanol to hydrocarbons, the pore size of the zeolites was reported to be crucial.[44] Longer chain hydrocarbons that are produced in a catalyst with small pores tend to block the pores and thereby decrease the overall selectivity for these hydrocarbons. On the contrary, zeolites with large pores should facilitate the production of C_{5+} hydrocarbons.[44] In addition, the acidic properties of the zeolites were determined by NH_3-TPD measurements. From the TPD profiles of the herein used materials (Figure 3), it can be derived that H-ZSM-5 provides weakly and strongly acidic sites, characterized by the desorption peaks at 194 and 368 °C with acid amounts of 0.078 and 0.22 mmol/g, respectively (Table 2). FAU-15 provides overall less acidic sites, which can be concluded from the significantly smaller desorption peak intensities compared to H-ZSM-5. This zeolite shows one broad signal at a temperature of 220 °C with a total acid amount of 0.14 mmol/g. The highest acidity is provided by Fe-BEA-35, which can be seen by the strong desorption peaks at 201 °C with an acid amount of 0.39 mmol/g for weakly acidic sites and at 367 °C with 0.66 mmol/g for strongly acidic sites. In general, high acidity is suggested to lead to the formation of more hydrogenated products and higher CO conversion, whereas low acidity zeolites lower the formation of coke and allow for the formation of an enhanced number of olefins.[38,45] Hence, we anticipated that Fe-BEA-35 provides the highest conversion to methane and paraffins, whereas FAU-15 should lead to the highest olefin selectivity among the tested zeolites.

Catalytic Performance over $Zn_aCr_bAl_cO_x$/H-ZSM-5. To determine the catalytic properties of the prepared composite catalysts and to identify a possible correlation of the Al content within the metal oxides and the catalytic activity, the combined oxide and zeolite materials were exposed to syngas under elevated temperature and pressure.

Figure 4 displays the hydrocarbon distribution for catalytic tests utilizing combinations of ZnCrAl oxides and a commercial H-ZSM-5 zeolite (see Figure S5 for a detailed product distribution) and the stability of the CO conversion and product selectivities is shown exemplarily in Figure S7 for

https://doi.org/10.1021/acsomega.2c05225
ACS Omega 2022, 7, 42994−43005

Table 2. N_2 Physisorption and Acidic Properties of the Zeolites

				NH_3-TPD				
				weakly acidic site		strongly acidic site		
zeolite	BET surface area (m^2/g)	total pore volume[a] (cm^3/g)	median pore width (nm)	temperature (°C)	acid amount (mmol/g)	temperature (°C)	acid amount (mmol/g)	total amount (mmol/g)
FAU-15	751	0.25	1.2	220	0.14			0.14
H-ZSM-5	468	0.08	0.88	194	0.078	368	0.22	0.298
Fe-BEA-35	597	0.17	0.96	201	0.39	367	0.66	1.05

[a]The total pore volume was determined at p/p_0 = 0.95.

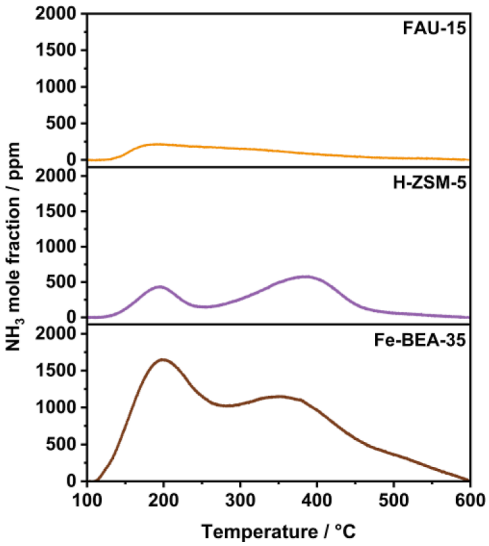

Figure 3. NH_3-TPD profiles of the zeolites.

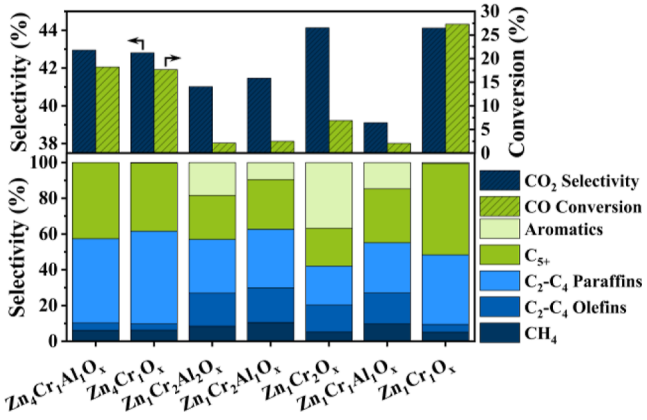

Figure 4. Hydrocarbon distribution, CO conversion, and CO_2 selectivity for catalytic tests of ZnCrAl oxides combined with H-ZSM-5. Reaction conditions: 400 °C, 2.5 MPa, 10,500 mL/g_{cat} h, $H_2/CO_2/N_2$ = 2/1/0.75, and at least 34 h time on stream (TOS).

$Zn_4Cr_1Al_1O_x$/H-ZSM-5. For $Zn_4Cr_1Al_cO_x$/H-ZSM-5 combinations, CO conversion and CO_2 selectivity remain almost constant with different equivalents of Al within the crystal lattice with conversion and selectivity values of 18 and 43% for both $Zn_4Cr_1O_x$ and $Zn_4Cr_1Al_1O_x$. Here, $Zn_4Cr_1Al_cO_x$ oxides as a component of the OX-ZEO catalyst mainly produce C_2-C_4 alongside C_{5+} paraffins, with selectivities of 52 and 38% for $Zn_4Cr_1O_x$ and 47 and 43% for $Zn_4Cr_1Al_1O_x$, respectively. Both $Zn_4Cr_1Al_cO_x$/H-ZSM-5 catalysts lead to the production of minor amounts of CH_4 with 6% selectivity and almost no aromatic compounds were observed. Instead, when $Zn_1Cr_2Al_cO_x$ oxides are applied along with H-ZSM-5, not only an overall significantly lower CO conversion but also a lower CO_2 selectivity is observed. In contrast to the oxides of the $Zn_4Cr_1Al_cO_x$ series, in the $Zn_1Cr_2Al_cO_x$ series the CO conversion decreases with increasing Al content from 6.9% for $Zn_1Cr_2O_x$/H-ZSM-5, over 2.5% for $Zn_1Cr_2Al_1O_x$/H-ZSM-5, down to 2.1% for $Zn_1Cr_2Al_2O_x$/H-ZSM-5. Notably, the CO_2 selectivity shows a similar trend and decreases from 44% down to 41% with increasing Al content. Likewise, the product distribution for the $Zn_1Cr_2Al_cO_x$/H-ZSM-5 combinations significantly differs from those of the $Zn_4Cr_1Al_cO_x$/H-ZSM-5 catalysts. Here, considerable amounts of C_2-C_4 olefins and aromatic compounds are formed. The highest selectivity for aromatics is reached using the combination of $Zn_1Cr_2O_x$ and H-ZSM-5 with 37%. In comparison to the other $Zn_1Cr_2Al_cO_x$ components, $Zn_1Cr_2O_x$/H-ZSM-5 produces the lowest amount of C_2-C_4 olefins with 15%, whereas $Zn_1Cr_2Al_1O_x$/H-ZSM-5 achieves the highest amount (19%). However, also for the $Zn_1Cr_2Al_cO_x$ oxides, the main products that were formed are C_2-C_4 paraffins with a selectivity ranging from 22% for $Zn_1Cr_2O_x$/H-ZSM-5 to 33% for $Zn_1Cr_2Al_1O_x$/H-ZSM-5. The enhanced selectivity toward paraffins for the $Zn_4Cr_1Al_cO_x$ components, if compared to the oxides with a Zn/Cr ratio of 1:2 can be explained by the presence of ZnO. ZnO is known to be active in hydrogenation processes and therefore is able to hydrogenate olefins that were produced over the zeolite.[19,21,45] Particularly interesting is the fact that not all abovementioned OX-XEO catalysts produce an aromatic fraction. This observation is quite unexpected, as similar reactions in the literature using a variety of different oxides combined with H-ZSM-5 reported aromatics to be the main product class.[16,26,27,34,35,42,46−53] As both components of the OX-ZEO catalyst affect the product distribution, it is crucial to fully understand the influence of each to be able to tailor the yields.

The hydrogenation ability of the oxide component has a strong impact on the product distribution of the OX-ZEO process.[23,45,52,53] This explains the higher paraffin selectivity, as well as the almost non-existent aromatic fraction for the $Zn_4Cr_1Al_cO_x$/H-ZSM-5 combinations because the olefins that serve as intermediates for the formation of aromatics also get hydrogenated over the ZnO component.[52,53] Contrarily, the $Zn_1Cr_1Al_cO_x$ oxides show a clearly different catalytic behavior. Although the hydrogenation ability of pure $Zn_4Cr_1Al_cO_x$ and $Zn_1Cr_2Al_cO_x$ does not differ strongly upon the incorporation of Al into the lattice, $Zn_1Cr_1Al_1O_x$/H-ZSM-5 and $Zn_1Cr_1O_x$/H-ZSM-5 lead to very different product distributions and CO conversion. Notably, the CO conversion over $Zn_1Cr_1Al_1O_x$/H-ZSM-5 was found to be 2.1%, whereas for $Zn_1Cr_1O_x$/H-ZSM-5 a value of 27% was observed. Also, the CO_2 selectivity changed notably from 39 to 44%. In addition, the combination of $Zn_1Cr_1O_x$ and H-ZSM-5 mainly yielded C_{5+} and C_2-C_4

https://doi.org/10.1021/acsomega.2c05225
ACS Omega 2022, 7, 42994−43005

paraffins with selectivities of 39% and 51%, respectively, and only 4.4% of C_2-C_4 olefins were formed. In stark contrast, $Zn_1Cr_1Al_1O_x$ enables a selectivity of 30% for C_{5+} hydrocarbons, 28% for C_2-C_4 paraffins, and 17% for C_2-C_4 olefins. The incorporation of one equivalent of Al into $Zn_1Cr_1O_x$ likewise leads to the formation of aromatic products, such as toluene and xylol (for further information, see Figure S5) with a selectivity of 15%.

Obviously, the distinct reactivity differences cannot be fully explained exclusively by the different hydrogenation abilities of the various oxides. Hence, it appears that other factors also play an important role in the conversion of syngas over the OX-ZEO catalyst. Along this line, DFT calculations conducted by Song et al. revealed that Zn-rich ZnCrO oxides consist of a thin ZnO-like layer supported on spinel-type $ZnCr_2O_4$.[54] This low-crystalline layer was found to be the active phase in the conversion of syngas to methanol. It was suggested that the formed oxygen vacancies are crucial for the activation of CO.[17,46,51,55] In addition, Wang et al. ascribed high importance to the $ZnO-ZnCr_2O_4$ interface in the conversion of syngas over a Zn_1Cr_1/SAPO-34 catalyst.[36] Here, the oxide with a Zn/Cr ratio of 1:1 showed the highest CO conversion and $C_2^=-C_4^=$ selectivity, which was attributed to an optimal interface between ZnO and $ZnCr_2O_4$. The CO conversion and hydrocarbon distribution for the combination of the different ZnCrAl oxides with H-ZSM-5 presented in this study align well with these findings. The $Zn_1Cr_1O_x$ oxide as a component of the OX-ZEO catalyst shows the highest CO conversion of all combinations, which can be explained by the facile formation of oxygen vacancies at the $ZnO-ZnCr_2O_4$ interface. $Zn_4Cr_1O_x$ with a Zn/Cr ratio of 4:1 should also provide a distinct $ZnO-ZnCr_2O_4$ interface, but the excess bulk ZnO hinders the oxygen vacancy formation, which leads to a lower CO conversion. Furthermore, $Zn_1Cr_2O_x$ is present in a pure spinel phase without an oxide−oxide interface and, accordingly, shows the lowest CO conversion. Obviously, the incorporation of Al into the oxides prevents the formation of the oxide−oxide interfaces, as $Zn_1Cr_1Al_1O_x$ in combination with the zeolite leads to the lowest conversion. This hypothesis is further supported by the N_2 sorption analysis, which showed a significant difference in BET surface area and total pore volume upon Al incorporation. Evidently, these observations support the strong influence of Al within the oxide lattice on structural properties. Furthermore, the difference in the hydrocarbon distribution between $Zn_1Cr_1Al_1O_x$/H-ZSM-5 and $Zn_1Cr_1O_x$/H-ZSM-5 suggests that the $ZnO-ZnCr_2O_4$ interface suppresses the formation of aromatics, presumably by hydrogenation of intermediate olefin species. From the overall product distribution (Figure S5), it becomes clear that the different metal ratios of the oxide components used for the syngas conversion not only affect the overall paraffin selectivity but also the degree of branching of the produced alkanes. The oxides with Zn/Cr = 1:2 mainly produce linear paraffins such as ethane and propane when combined with H-ZSM-5, whereas the $Zn_4Cr_1Al_cO_x$/H-ZSM-5 combinations also produce significant amounts of the branched alkanes 2-methylpropane (5.6−6.7%), 2-methylbutane (11%), and 2-methylpentane (4.7−5.2%). Again, the $Zn_1Cr_1Al_cO_x$ oxides differ notably from each other. While $Zn_1Cr_1O_x$/H-ZSM-5 shows high amounts of 2-methylpropane, 2-methylbutane, and 2-methylpentane, $Zn_1Cr_1O_x$/H-ZSM-5 mainly produces the linear alkanes ethane, propane, and hexane. This further supports the importance of composition and structural properties of the oxide component of the OX-ZEO catalysts for the hydrocarbon distribution. The collected product distribution data suggest a more complicated reaction mechanism and not a simple combination of methanol synthesis over the oxide and subsequent methanol-to-hydrocarbons conversion over the zeolite. If this was the case, different oxides should mainly affect the CO conversion, according to their ability to synthesize methanol, and the paraffin/olefin ratio, according to their hydrogenation ability. Hence, the differences in the hydrocarbon distribution for the different oxide components that extend the expected differences due to differing hydrogenation abilities indicate that the role of the oxide is not limited to the conversion of syngas to methanol. In close proximity to the zeolite, the oxides might also produce other intermediates than methanol, such as ketene or dimethyl ether, that are converted to different products over the zeolite. If differences in the composition and surface properties of the oxide component of the OX-ZEO process led to different reaction intermediates, which in turn led to different reaction products, this would also explain the different findings in the literature concerning the intermediate, as these studies were performed using different oxide materials.[14,21,23]

Influence of the Zeolite. Next to the metal ratio of the oxide component, the influence of the used zeolite on the catalytic properties of the bifunctional catalyst was studied.

In Figure 5, the hydrocarbon distribution, CO conversion, and CO_2 selectivity for $Zn_4Cr_1Al_1O_x$ combined with the commercial zeolites H-ZSM-5, FAU-15, and Fe-BEA-35 are shown. Combining $Zn_4Cr_1Al_1O_x$ with FAU-15 led to the formation of lower olefins, lower paraffins, and C_{5+} hydrocarbons with 41, 21, and 22%, respectively. The observed selectivity for methane was 14% with an overall selectivity for CO_2 of 43%. Compared to H-ZSM-5, the olefin selectivity for the FAU-15-containing catalyst is notably higher. Interestingly, N_2 physisorption properties do not correlate with the hydrocarbon distribution, as the larger pores in FAU-15 and Fe-BEA-35 were expected to facilitate the diffusion of longer chain hydrocarbons that were produced inside the zeolite's pores with an elevated generation of C_{5+} species. The maximum selectivity of 43% for C_{5+} hydrocarbons, however, can be observed for H-ZSM-5 that provides the smallest pore volume and width. Furthermore, the overall conversion was expected to increase parallel to the surface area. Yet, the

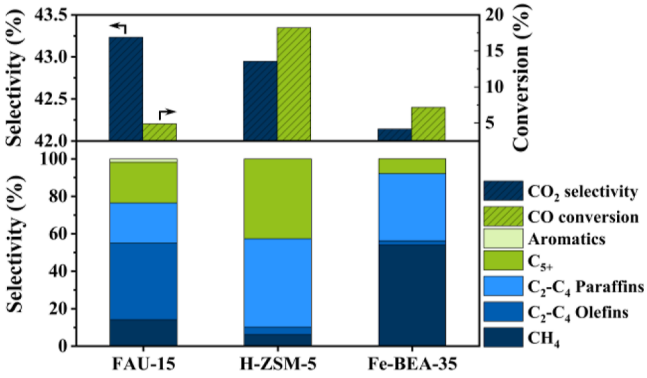

Figure 5. Hydrocarbon distribution, CO conversion, and CO_2 selectivity for catalytic tests of $Zn_4Cr_1Al_1O_x$ combined with several zeolites. Reaction conditions: 400 °C, 2.5 MPa, 10,500 mL/g_{cat} h, $H_2/CO_2/N_2$ = 2/1/0.75, and at least 34 h TOS.

https://doi.org/10.1021/acsomega.2c05225
ACS Omega 2022, 7, 42994−43005

highest surface area of 751 m^2/g for FAU-15 led to the lowest CO conversion of 4.9% and the lowest surface area of 468 m^2/g for H-ZSM-5 led to the highest CO conversion of 18%. From the product distribution of $Zn_4Cr_1Al_1O_x$/FAU-15 and $Zn_4Cr_1Al_1O_x$/Fe-BEA-35 (Figure S6), it can obviously be deduced that the low CO conversion for these combinations is accompanied by an excess of methanol and dimethyl ether that could not be further converted by the zeolite. This can be explained by the strong influence of the ring size of the zeolite pores on the conversion of the intermediates in the OX-ZEO process.[37,47]

H-ZSM-5 (MFI framework) provides 10-membered rings, whereas FAU-15 (FAU framework) and Fe-BEA-35 (BEA framework) both have 12-membered rings (Figure 6), which in

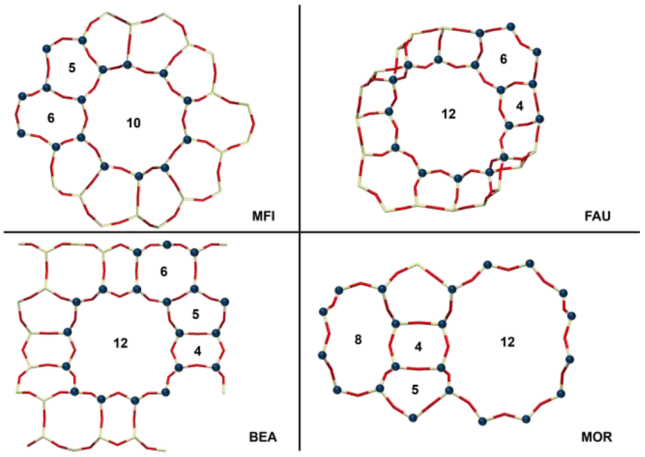

Figure 6. Ring sizes of zeolite framework types.

both cases lead to very low CO conversions. Jiao et al. observed a similar trend when they studied the catalytic activity of a combination of $ZnCrO_x$ and mordenite (MOR framework).[20] In their study, they showed that in combination with an oxide material, a mordenite that contains 8- and 12-membered rings reached a lower CO conversion than a mordenite where the 12-membered rings are blocked. Jiao et al. were able to demonstrate that ketene mostly adsorbs in the channels with 8-membered rings, whereas methanol primarily adsorbs in the 12-membered rings. This behavior suggests that the reaction takes place via a different mechanism in channels with 8- and 12-membered rings and proceeds faster for the ketene pathway in pores with 8-membered rings. Furthermore, the acidity of the zeolite materials plays a crucial role in the product distribution. The weak acidity and small number of acidic sites of the FAU-15 zeolite favor the production of olefins, as the hydrogenation of unsaturated hydrocarbons by strong acidic sites is less likely to occur over this catalyst if compared to H-ZSM-5 and Fe-BEA-35. For $Zn_4Cr_1Al_1O_x$/Fe-BEA-35, a $C_2^=-C_4^=$ selectivity of 2.4% alongside a $C_2^0-C_4^0$ selectivity of 36% and a methane selectivity of 54% was reached. The high amount of weakly and highly acidic sites in Fe-BEA-35 explains the high methane selectivity, as the acidic sites over-hydrogenate the intermediate that was previously produced over the oxide to form CH_4.

In Figure 7, the PXRD patterns of the spent composite catalysts with different zeolites are shown. These patterns demonstrate that the phases of the oxides and zeolites remain unchanged under the applied reaction conditions. The stability

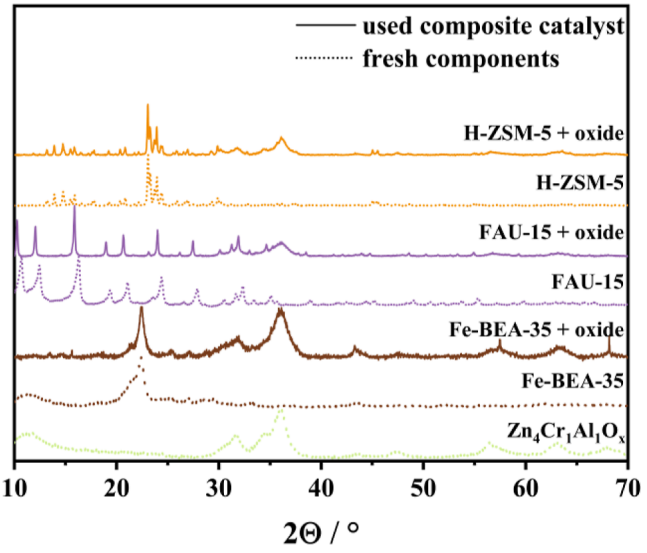

Figure 7. PXRD patterns of the composite catalyst after the reaction. Reaction conditions: 400 °C, 2.5 MPa, 10,500 mL/g_{cat} h, $H_2/CO_2/N_2$ = 2/1/0.75, and at least 34 h TOS. The mass ratio of oxide/zeolite = 1:1.

of the phases for all of the tested oxide materials can be seen in Figure S4.

Influence of Space Velocity. In addition to the nature of the oxide and zeolite components, the reaction parameters pressure, temperature, and space velocity are other important factors for the conversion of syngas to hydrocarbons. Due to the bifunctional nature of the OX-ZEO catalyst, the reaction parameters must be optimized to find sweet spots for both processes that take place. Here, the influence of the gas hourly space velocity (GHSV) on the product distribution and the CO conversion was studied using the bifunctional catalyst composed of $Zn_4Cr_1Al_1O_x$ and H-ZSM-5.

Figure 8 shows the hydrocarbon distribution, CO_2 selectivity, and CO conversion at four different space velocities. The influence of the GHSV on the reaction appears to increase drastically with decreasing velocity. The reduction of the GHSV by half from 21,000 ml/g_{cat} h to 10,500 ml/$_{gcat}$ h causes only small changes in product selectivities and conversion. However, further decreasing the space velocity to

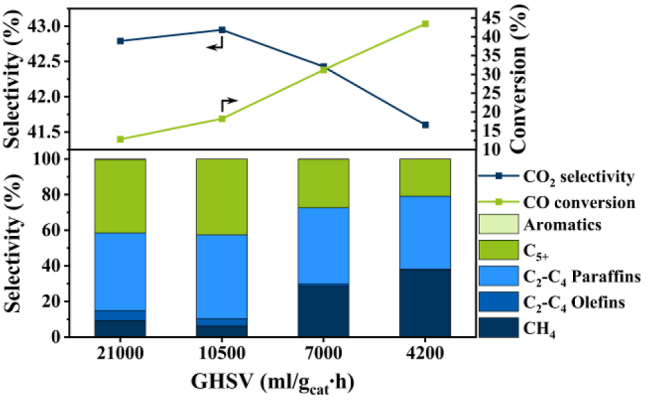

Figure 8. Hydrocarbon distribution, CO conversion, and CO_2 selectivity for catalytic tests of $Zn_4Cr_1Al_1O_x$/H-ZSM-5 tested at different GHSV. Reaction conditions: 400 °C, 2.5 MPa, $H_2/CO_2/N_2$ = 2/1/0.75, and at least 34 h TOS.

https://doi.org/10.1021/acsomega.2c05225
ACS Omega 2022, 7, 42994−43005

7000 mL/g_{cat} h has a significant effect on the reaction. The CO conversion increases strongly from 18 to 31%, while the $C_2^=-C_4^=$ selectivity decreases from 4.1 to 1.2%, and the C_{5+} selectivity decreases from 43 to 27%. The methane selectivity at 10,500 mL/g_{cat} h reaches only 6.1%, whereas at 7000 mL/g_{cat} h already 29% of the formed hydrocarbons are methane. A further decrease in the GHSV from 7000 to 4200 mL/g_{cat} h leads to a further increase in methane selectivity to 38%, and a further decrease in $C_2^=-C_4^=$, C_2-C_4 paraffin and C_{5+} selectivities. The CO conversion at 4200 mL/g_{cat} h was found to be as high as 44%, which is among the highest values reached by OX-ZEO catalysts in the current literature.[14−25,28−42,45−47,49,52,53,55−59] The increasing conversion is caused by the higher contact time, which also leads to enhanced hydrogenation of the hydrocarbons. A correlation between GHSV and CO_2 formation was not observed, as for all space velocities tested in this study a CO_2 selectivity of around 42% was observed.

Oxide Composition−Activity Relationship. The tested oxide−zeolite combinations revealed a strong influence of the composition of the oxide material on the catalytic activity and the product distribution of the OX-ZEO process. The ZnO component in the oxide part of the composite catalyst was shown to hydrogenate olefins that were primarily produced by the zeolite, leading to high paraffin selectivity. In addition, ZnO can hydrogenate olefin intermediates that otherwise would be converted to aromatic products. Hence, for OX-ZEO catalysts with a ZnO-rich oxide component, only minor olefin and aromatics selectivities are observed. Furthermore, the mixed phase of ZnO and spinel in the $Zn_4Cr_1Al_cO_x$ oxides provides a high CO conversion if combined with H-ZSM-5. The pure spinel structure in $Zn_1Cr_2Al_cO_x$ has lower hydrogenation ability and therefore allows production of olefins and an aromatic fraction in the OX-ZEO process. The incorporation of Al into the oxide has no significant effect on the catalytic behavior for the $Zn_4Cr_1O_x$ oxide, as can be seen from the similar yields utilizing $Zn_4Cr_1Al_1O_x$. This observation is in line with the small structural changes that were observed by PXRD and XPS. However, for the pure spinel oxide $Zn_1Cr_2O_x$, the addition of Al leads to a notable change in both the CO conversion and the product distribution. For oxides that contain one equivalent of Al, the aromatics selectivity decreases in favor of the paraffin and olefin selectivity. If the formation of aromatics was hindered by hydrogenation processes similar to those occurring over ZnO, the olefin selectivity would decrease accordingly. However, the $C_2^=-C_4^=$ selectivity increases upon the incorporation of Al, suggesting a more important contribution of the oxide component. A possible explanation for this phenomenon could be that on Al^{3+}-exposing oxide surfaces the production of other intermediates is favored compared to the sole ZnCr oxides. This hypothesis is supported by the findings of Lai et al. who revealed a strong connection between the surface binding site (oxygen vacancy, metal atom, or combinations of these) and the favored reaction product (methanol, ketene, or methane).[60] Since Wang et al. pointed out the differences in the reaction mechanism of the conversion of ketene and methanol over a zeolite, it is likely that the two intermediates lead to different products.[61] The introduction of two equivalents of Al into $Zn_1Cr_2O_x$ to form $Zn_1Cr_2Al_2O_x$ resulted in only small changes, as mainly the selectivity of aromatics decreased in favor of other hydrocarbons. This trend is in line with the finding that the structural features of $Zn_1Cr_2Al_1O_x$ do not differ strongly upon the introduction of a second Al equivalent. A particularly strong correlation between catalytic activity and surface structure was observed for the $Zn_1Cr_1Al_cO_x$ oxides. Here, the binary $Zn_1Cr_1O_x$ oxide offers a surface consisting of a low-crystalline ZnO layer. This layer influences the activity of the composite catalyst in such a way that a high CO conversion and mainly saturated hydrocarbons are obtained. However, upon the addition of one equivalent of Al during the synthesis to form $Zn_1Cr_1Al_1O_x$, the low-crystalline ZnO layer seems to collapse, which drastically changes the reaction results for the OX-ZEO process. The hydrocarbon distribution for $Zn_1Cr_1Al_1O_x$/H-ZSM-5 is very similar to the one obtained with $Zn_1Cr_2Al_1O_x$/H-ZSM-5, suggesting very similar structural features. This hypothesis seems plausible, as Al^{3+} can replace Cr^{3+} in the lattice of $Zn_1Cr_1Al_1O_x$, which then would give a stoichiometric composition for the spinel $Zn(Cr/Al)_2O_4$. As the same metal species are present in the spinel-type oxide $Zn_1Cr_2Al_1O_x$, these oxides should provide similar binding sites for CO and H_2 and therefore lead to similar intermediates. By taking the XPS analysis into account, it is noticeable that the change in binding energy due to the introduction of Al correlates with the influence of Al on the reaction results. For the oxides where the Al addition resulted in an increase in the O 1s and Cr 2p binding energies of the surface atoms ($Zn_1Cr_2Al_cO_x$, $Zn_1Cr_1Al_cO_x$), Al also has a significant effect on the conversion and product selectivities in the OX-ZEO process. In the case of $Zn_4Cr_1Al_cO_x$, however, the incorporation of Al resulted in lower binding energies and hardly any influence on the reaction results. This indicates that Al plays a more important role in the adsorption of the reagents in the spinel phase than it does in the ZnO phase. The observed effect of Al when added to the oxide directly during the synthesis is notably larger than it would be expected for a sole mixture of ZnCr oxide with α-Al_2O_3. Hence, the addition of Al^{3+} into the synthesis mixture of the oxide material is a valuable tool to steer the reactivity of this catalyst component.

CONCLUSIONS

A series of ZnCrAl oxides with varying metal ratios was synthesized as one component of a bifunctional composite catalyst and combined with commercial zeolite materials for the direct conversion of syngas to hydrocarbons. The composition and surface structure of the oxide material were identified to play a crucial role in this conversion, as a pure spinel $Zn_1Cr_2O_x$ oxide combined with H-ZSM-5 provides the highest values for the production of aromatics, whereas $Zn_4Cr_1O_x$, a mixed metal oxide consisting of ZnO and $ZnCr_2O_4$, produces almost no aromatic fraction but the highest amount of C_2-C_4 alkanes. A thin, low-crystalline ZnO layer on top of the $ZnCr_2O_4$ phase, present in $Zn_1Cr_1O_x$ is assumed to provide high hydrogenation ability, as almost no olefins or aromatics were observed over $Zn_1Cr_1O_x$/H-ZSM-5. The introduction of Al into the binary ZnCr oxides during the synthesis was shown to have a significant effect on the OX-ZEO process. In $Zn_1Cr_1Al_1O_x$, Al appeared to hinder the formation of the ZnO−$ZnCr_2O_4$ interface, as this oxide showed a similar hydrocarbon distribution as the pure spinel oxides. Additionally, the CO conversion was shown to be strongly correlated to the metal ratio of the oxides. The incorporation of Al and the variation of the metal ratio in the oxide component were shown to provide a possibility to tailor the product distribution of the OX-ZEO process, whether these are paraffins or olefinic and aromatic compounds,

https://doi.org/10.1021/acsomega.2c05225
ACS Omega 2022, 7, 42994−43005

respectively. Next to the oxide, the zeolite component also has a strong influence on both product selectivity and CO conversion. H-ZSM-5 was shown to provide the highest CO conversion and paraffin selectivity due to its optimal topology and acidic properties. FAU-15 was found to be the most suitable zeolite material to produce lower olefins in combination with $Zn_4Cr_1Al_1O_x$. Fe-BEA-35 together with $Zn_4Cr_1Al_1O_x$ was shown to mainly produce methane, caused by the high number of acidic sites that lead to an over-hydrogenation of produced hydrocarbons. The variation of the GHSV indicated that a higher contact time leads to an enhanced CO conversion and hydrogenation of formed hydrocarbons. At a GHSV of 4200 ml/g_{cat} h, the highest CO conversion of 43.5% was observed together with a C_2^0−C_4^0 selectivity of 40.9%, a C_{5+} selectivity of 20.9%, a CH_4 selectivity of 37.6%, and a CO_2 selectivity of 41.6%. All tested catalyst combinations were shown to retain their structure under the applied reaction conditions by PXRD analysis after the reaction. The results presented herein point toward a reaction mechanism that proceeds via different reaction intermediates for different oxide components. To fully understand the OX-ZEO process and its advantages over the separate methanol synthesis and methanol-to-hydrocarbons processes, the differences in the reaction intermediate over various oxide materials should be studied in more detail in the future.

EXPERIMENTAL SECTION

Materials. If not otherwise stated, all chemicals were obtained from commercial vendors and used without further purification. In particular, H-ZSM-5 was obtained from Clariant (product name: TZP1524, SiO_2/Al_2O_3 = 150), FAU-15 was purchased from Tosoh (product name: 360-HUA, SiO_2/Al_2O_3 = 15), and Fe-BEA-35 from Tricat (product name: Fe-TZB223L, SiO_2/Al_2O_3 = 35).

Preparation of $Zn_aCr_bAl_cO_x$. ZnCrAl oxides with different metal ratios were prepared following the method reported by Jiao et al.[14] The Zn, Cr, and Al nitrates were dissolved in deionized water in the desired molar ratios and stirred for 1 h at 70 °C. Subsequently, a 2 M aqueous $(NH_4)_2CO_3$ solution was added. The formed precipitate was filtered off, washed several times with deionized water, dried at 120 °C, and calcined at 450 °C for 3 h under air atmosphere. The oxide materials are denoted as $Zn_aCr_bAl_cO_x$ (with *abc* representing the metal ratio of *a*: Zn; *b*: Cr; *c*: Al and *a* = 1, 4; *b* = 1, 2; for *b* = 1 → *c* = 0, 1; for *b* = 2 → *c* = 0, 1, 2).

Preparation of the Composite Catalyst. The corresponding oxide and zeolite material were mixed with a mass ratio of 1:1 and ground for 10 min in an agate mortar. The resulting mixture was then pressed to pellets that were crushed over sieves with a mesh size of 35−60 mesh to obtain a powder with a defined grain size to prevent problems due to too fine powder in the flow reactor.[35,46,55]

Catalyst Characterization. PXRD measurements were performed on a Bruker D2 Phaser diffractometer equipped with a LynxEye detector operating at 30 kV acceleration voltage and 10 mA emission current using Cu Kα radiation (λ = 1.54184 Å). The data were recorded in a range from 10 to 70° 2θ. XPS analysis was carried out on a Nexsa G2 surface analysis system with a monochromared, micro-focused, focused, high-efficiency Al Kα X-ray source. The analyzer used was a 180°, double-focusing, hemispherical analyzer with a 128-channel detector. A 400 μm spot was analyzed with a pass energy of 200.0 eV and a step size of 0.100 eV. The results were calibrated based on the carbon signal at 284.8 eV and evaluated using CasaXPS software (version 2.3.15). Scanning electron microscopy (SEM) was performed on a ZEISS Gemini2 Merlin HR-FESEM equipped with an OXFORD AZtecEnergy X-ray microanalysis system for EDX. The SEM images and EDX mapping were recorded at an acceleration voltage of 20 kV. HR-TEM was carried out with a JEOL JEM 2800 microscope that was equipped with a Schottky-type emission source working at 200 kV. Images were taken with a Gatan OneView camera (4k × 4k, 25 FPS) with a resolution of 0.09 nm. N_2 physisorption experiments were conducted on a Micromeritics 3Flex version 5.02 at −196 °C after degassing the sample under vacuum for 60 min at 30 °C. Temperature-programmed desorption of NH_3 (NH_3-TPD) was conducted by placing 100 mg of the sample in a U-shaped quartz reactor between to quartz wool plugs. The reactor was fixed between to steel plates that are heated by two heating cartridges. The reactor was flushed with inert gas at 30 ml/min for 10 min at room temperature and then heated to 573.15 K with a heating ramp of 5 K/min. Subsequently, the reactor was cooled down to 373.15 K and it was flushed for another 100 min. The gas feed was then switched to 2500 ppm NH_3 in He, which was adsorbed for about 2.5 h and flushed out again by pure He for 2 h. Finally, the reactor was heated from 373.15 to 873.15 K with a linear heating ramp of 5 K/min. The effluent gas stream was analyzed with a four-channel Rosemount NGA 2000 from Emerson Electric Co., USA that detects NH_3 in the range of 0 to 5000 ppm and does not detect water, so that only the acidic sites of the sample are probed.

Catalyst Testing. Catalytic reactions were performed in a continuous flow, fixed-bed stainless-steel reactor with eight parallel reactors. About 200−500 mg of the catalyst was filled in the reactor and diluted with inert aluminum oxide. The catalysts were in situ reduced under a H_2 atmosphere prior to the test at room temperature for 16 h. The reaction was conducted under a $H_2/CO_2/N_2$ atmosphere with a ratio of 2/1/0.75. The reaction temperature was set to 400 °C, the pressure to 2.5 MPa, and the GHSV to 10,500 mL/g_{cat} h unless otherwise stated. Reaction products were analyzed with an online GC equipped with a thermal conductivity detector and a flame ionization detector with a HP-Plot/Q + PT column after at least 34 h TOS. N_2 was used as an internal standard and the carbon balance always exceeded 95%. The CO conversion (X_{CO}) was calculated on a carbon atom basis following the equation

$$X_{CO} = \frac{\dot{n}_{CO,in} - \dot{n}_{CO,out}}{\dot{n}_{CO,in}} \times 100\%$$

where $\dot{n}_{CO,in}$ is the ingoing and $\dot{n}_{CO,out}$ is the outgoing CO molar flow. The CO_2 selectivity (S_{CO_2}) was calculated according to the following equation

$$S_{CO_2} = \frac{\dot{n}_{CO_2,out}}{\dot{n}_{CO,in} - \dot{n}_{CO,out}} \times 100\%$$

where $\dot{n}_{CO_2,out}$ is the outgoing molar flow of CO_2.The selectivity for the individual hydrocarbons ($S_{C_iH_j}$) was calculated according to the following equation

https://doi.org/10.1021/acsomega.2c05225
ACS Omega 2022, 7, 42994−43005

$$S_{C_iH_j} = \frac{\dot{n}_{i_iH_j,out}}{\sum_{i=1}^{n} \dot{n}_{C_iH_j,out}} \times 100\%$$

where $\dot{n}_{C_iH_j,out}$ represents the effluent molar flow of the corresponding hydrocarbon.

■ ASSOCIATED CONTENT

Supporting Information

The Supporting Information is available free of charge at https://pubs.acs.org/doi/10.1021/acsomega.2c05225.

XPS analysis; SEM, EDX mapping, and HR-TEM images of synthesized oxides; PXRD patterns of spent composite catalysts; and detailed data of the catalytic performance (PDF)

■ AUTHOR INFORMATION

Corresponding Author

Ulf-Peter Apfel − *Inorganic Chemistry I, Ruhr-Universität Bochum, D-44780 Bochum, Germany; Fraunhofer UMSICHT, D-46047 Oberhausen, Germany;* orcid.org/0000-0002-1577-2420; Phone: 49(0)234 32-21831; Email: ulf.apfel@rub.de

Authors

Tobias Kull − *Inorganic Chemistry I, Ruhr-Universität Bochum, D-44780 Bochum, Germany*

Thomas Wiesmann − *Fraunhofer UMSICHT, D-46047 Oberhausen, Germany*

Andrea Wilmsen − *Fraunhofer UMSICHT, D-46047 Oberhausen, Germany*

Maximilian Purcel − *Laboratory of Industrial Chemistry, Ruhr-Universität Bochum, D-44780 Bochum, Germany;* orcid.org/0000-0003-0252-6607

Martin Muhler − *Laboratory of Industrial Chemistry, Ruhr-Universität Bochum, D-44780 Bochum, Germany;* orcid.org/0000-0001-5343-6922

Heiko Lohmann − *Fraunhofer UMSICHT, D-46047 Oberhausen, Germany*

Barbara Zeidler-Fandrich − *Fraunhofer UMSICHT, D-46047 Oberhausen, Germany*

Complete contact information is available at: https://pubs.acs.org/10.1021/acsomega.2c05225

Notes

The authors declare no competing financial interest.

■ ACKNOWLEDGMENTS

We are grateful for the financial support from the Fraunhofer Internal Programs under Grant No. Attract 097-602175 and the Doctoral School Closed Carbon Cycle Economy. The project DS CCCE is funded by the State of North Rhine-Westphalia through the Ministry of Economic Affairs, Innovation, Digitalization, and Energy of the State of North Rhine-Westphalia (MWIDE NRW).

■ REFERENCES

(1) Schulz, H. Short history and present trends of Fischer−Tropsch synthesis. *Appl. Catal., A* **1999**, *186*, 3−12.

(2) Mittasch, A.; Schneider, C. Producing Compounds Containing Carbon and Hydrogen. U.S. Patent 1,201,850 A, 1916.

(3) Mittasch, A.; Pier, M. Synthetic Manufacture of Methanol. U.S. Patent 1,569,775 A, 1926.

(4) Fischer, F.; Tropsch, H. Verfahren zur Gewinnung mehrgliedriger Paraffinkohlenwasserstoffe aus Kohlenoxyden und Wasserstoff auf katalytischem Wege. DE 484337 C, 1929.

(5) Centi, G.; Perathoner, S. Chemistry and energy beyond fossil fuels. A perspective view on the role of syngas from waste sources. *Catal. Today* **2020**, *342*, 4−12.

(6) Foit, S. R.; Vinke, I. C.; de Haart, L. G. J.; Eichel, R.-A. Power-to-Syngas: An Enabling Technology for the Transition of the Energy System? *Angew. Chem., Int. Ed. Engl.* **2017**, *56*, 5402−5411.

(7) Bian, L.; Duan, C.; Wang, L.; Chen, Z.; Hou, Y.; Peng, J.; Song, X.; An, S.; O'Hayre, R. An all-oxide electrolysis cells for syngas production with tunable H2/CO yield via co-electrolysis of H2O and CO2. *J. Power Sources* **2021**, *482*, 228887.

(8) Siegmund, D.; Metz, S.; Peinecke, V.; Warner, T. E.; Cremers, C.; Grevé, A.; Smolinka, T.; Segets, D.; Apfel, U.-P. Crossing the Valley of Death: From Fundamental to Applied Research in Electrolysis. *JACS Au* **2021**, *1*, 527−535.

(9) Hoof, L.; Thissen, N.; Pellumbi, K.; junge Puring, K.; Siegmund, D.; Mechler, A.; Apfel, U.-P. Press it, Heat it, Twist it: A Series of Hidden Parameters for the Electrochemical CO $_2$ Reduction in Zero-Gap Electrolyzers. *SSRN Journal* **2021**, DOI: 10.2139/ssrn.3991077.

(10) Friedel, R. A.; Anderson, R. B. Composition of Synthetic Liquid Fuels. I. Product Distribution and Analysis of C5-C8 Paraffin Isomers from Cobalt Catalyst1. *J. Am. Chem. Soc.* **1950**, *72*, 1212−1215.

(11) Nakhaei Pour, A.; Housaindokht, M. R. Studies on product distribution of nanostructured iron catalyst in Fischer-Tropsch synthesis: Effect of catalyst particle size. *J. Ind. Eng. Chem.* **2014**, *20*, 591−596.

(12) Albuquerque, J. S.; Costa, F. O.; Barbosa, B. V. S. Fischer-Tropsch Synthesis: Analysis of Products by Anderson-Schulz-Flory Distribution Using Promoted Cobalt Catalyst. *Catal. Lett.* **2019**, *149*, 831−839.

(13) Chang, C. D.; Lang, W. H.; Silvestri, A. J.; Smith, R. L. Conversion of Synthesis Gas to Hydrocarbon Mixtures. U.S. Patent 4,096,163 A, 1978.

(14) Jiao, F.; Li, J.; Pan, X.; Xiao, J.; Li, H.; Ma, H.; Wei, M.; Pan, Y.; Zhou, Z.; Li, M.; Miao, S.; Li, J.; Zhu, Y.; Xiao, D.; He, T.; Yang, J.; Qi, F.; Fu, Q.; Bao, X. Selective conversion of syngas to light olefins. *Science* **2016**, *351*, 1065−1068.

(15) Zhu, Y.; Pan, X.; Jiao, F.; Li, J.; Yang, J.; Ding, M.; Han, Y.; Liu, Z.; Bao, X. Role of Manganese Oxide in Syngas Conversion to Light Olefins. *ACS Catal.* **2017**, *7*, 2800−2804.

(16) Zhou, W.; Shi, S.; Wang, Y.; Zhang, L.; Wang, Y.; Zhang, G.; Min, X.; Cheng, K.; Zhang, Q.; Kang, J.; Wang, Y. Selective Conversion of Syngas to Aromatics over a Mo−ZrO 2 /H-ZSM-5 Bifunctional Catalyst. *ChemCatChem* **2019**, *11*, 1681−1688.

(17) Liu, X.; Wang, M.; Yin, H.; Hu, J.; Cheng, K.; Kang, J.; Zhang, Q.; Wang, Y. Tandem Catalysis for Hydrogenation of CO and CO2 to Lower Olefins with Bifunctional Catalysts Composed of Spinel Oxide and SAPO-34. *ACS Catal.* **2020**, *10*, 8303−8314.

(18) Su, J.; Wang, D.; Wang, Y.; Zhou, H.; Liu, C.; Liu, S.; Wang, C.; Yang, W.; Xie, Z.; He, M. Direct Conversion of Syngas into Light Olefins over Zirconium-Doped Indium(III) Oxide and SAPO-34 Bifunctional Catalysts: Design of Oxide Component and Construction of Reaction Network. *ChemCatChem* **2018**, *10*, 1536−1541.

(19) Meng, F.; Li, X.; Zhang, P.; Yang, L.; Yang, G.; Ma, P.; Li, Z. Highly active ternary oxide ZrCeZnOx combined with SAPO-34 zeolite for direct conversion of syngas into light olefins. *Catal. Today* **2020**, *368*, 118−125.

(20) Jiao, F.; Pan, X.; Gong, K.; Chen, Y.; Li, G.; Bao, X. Shape-Selective Zeolites Promote Ethylene Formation from Syngas via a Ketene Intermediate. *Angew. Chem., Int. Ed. Engl.* **2018**, *57*, 4692−4696.

(21) Liu, X.; Zhou, W.; Yang, Y.; Cheng, K.; Kang, J.; Zhang, L.; Zhang, G.; Min, X.; Zhang, Q.; Wang, Y. Design of efficient bifunctional catalysts for direct conversion of syngas into lower olefins via methanol/dimethyl ether intermediates. *Chem. Sci.* **2018**, *9*, 4708−4718.

(22) Su, J.; Zhou, H.; Liu, S.; Wang, C.; Jiao, W.; Wang, Y.; Liu, C.; Ye, Y.; Zhang, L.; Zhao, Y.; Liu, H.; Wang, D.; Yang, W.; Xie, Z.; He, M. Syngas to light olefins conversion with high olefin/paraffin ratio using ZnCrOx/AlPO-18 bifunctional catalysts. *Nat. Commun.* **2019**, *10*, 2130.
(23) Zhang, P.; Meng, F.; Li, X.; Yang, L.; Ma, P.; Li, Z. Excellent selectivity for direct conversion of syngas to light olefins over a Mn-Ga oxide and SAPO-34 bifunctional catalyst. *Catal. Sci. Technol.* **2019**, *9*, 5577−5581.
(24) Ni, Y.; Liu, Y.; Chen, Z.; Yang, M.; Liu, H.; He, Y.; Fu, Y.; Zhu, W.; Liu, Z. Realizing and Recognizing Syngas-to-Olefins Reaction via a Dual-Bed Catalyst. *ACS Catal.* **2019**, *9*, 1026−1032.
(25) Tan, L.; Wang, F.; Zhang, P.; Suzuki, Y.; Wu, Y.; Chen, J.; Yang, G.; Tsubaki, N. Design of a core-shell catalyst: an effective strategy for suppressing side reactions in syngas for direct selective conversion to light olefins. *Chem. Sci.* **2020**, *11*, 4097−4105.
(26) Yang, S.; Li, M.; Nawaz, M. A.; Song, G.; Xiao, W.; Wang, Z.; Liu, D. High Selectivity to Aromatics by a Mg and Na Co-modified Catalyst in Direct Conversion of Syngas. *ACS Omega* **2020**, *5*, 11701−11709.
(27) Zhou, W.; Zhou, C.; Yin, H.; Shi, J.; Zhang, G.; Zheng, X.; Min, X.; Zhang, Z.; Cheng, K.; Kang, J.; Zhang, Q.; Wang, Y. Direct conversion of syngas into aromatics over a bifunctional catalyst:Inhibiting net CO 2 release. *Chem. Commun.* **2020**, *3*, 198.
(28) Huang, Y.; Ma, H.; Xu, Z.; Qian, W.; Zhang, H.; Ying, W. Role of nanosized sheet-like SAPO-34 in bifunctional catalyst for syngas-to-olefins reaction. *Fuel* **2020**, *273*, 117771.
(29) Wang, S.; Wang, P.; Shi, D.; He, S.; Zhang, L.; Yan, W.; Qin, Z.; Li, J.; Dong, M.; Wang, J.; Olsbye, U.; Fan, W. Direct Conversion of Syngas into Light Olefins with Low CO2 Emission. *ACS Catal.* **2020**, *10*, 2046−2059.
(30) Huang, Y.; Ma, H.; Xu, Z.; Qian, W.; Zhang, H.; Ying, W. Direct Conversion of Syngas to Light Olefins over a ZnCrOx + H-SSZ-13 Bifunctional Catalyst. *ACS Omega* **2021**, *6*, 10953−10962.
(31) Huang, Y.; Ma, H.; Xu, Z.; Qian, W.; Zhang, H.; Ying, W. Utilization of SAPO-18 or SAPO-35 in the bifunctional catalyst for the direct conversion of syngas to light olefins. *RSC Adv.* **2021**, *11*, 13876−13884.
(32) Kirilin, A. V.; Dewilde, J. F.; Santos, V.; Chojecki, A.; Scieranka, K.; Malek, A. Conversion of Synthesis Gas to Light Olefins: Impact of Hydrogenation Activity of Methanol Synthesis Catalyst on the Hybrid Process Selectivity over Cr-Zn and Cu-Zn with SAPO-34. *Ind. Eng. Chem. Res.* **2017**, *56*, 13392−13401.
(33) Su, J.; Liu, C.; Liu, S.; Ye, Y.; Du, Y.; Zhou, H.; Liu, S.; Jiao, W.; Zhang, L.; Wang, C.; Wang, Y.; Xie, Z. High Conversion of Syngas to Ethene and Propene on Bifunctional Catalysts via the Tailoring of SAPO Zeolite Structure. *Cell Rep. Phys. Sci.* **2021**, *2*, 100290.
(34) Zhang, P.; Tan, L.; Yang, G.; Tsubaki, N. One-pass selective conversion of syngas to para-xylene. *Chem. Sci.* **2017**, *8*, 7941−7946.
(35) Arslan, M. T.; Qureshi, B. A.; Gilani, S. Z. A.; Cai, D.; Ma, Y.; Usman, M.; Chen, X.; Wang, Y.; Wei, F. Single-Step Conversion of H2-Deficient Syngas into High Yield of Tetramethylbenzene. *ACS Catal.* **2019**, *9*, 2203−2212.
(36) Wang, X.; Cao, R.; Chen, K.; Si, C.; Ban, H.; Zhang, P.; Meng, F.; Jia, L.; Mi, J.; Li, Z.; Li, C. Synthesis Gas Conversion to Lower Olefins over ZnCr-SAPO-34 Catalysts: Role of ZnO−ZnCr 2 O 4 Interface. *ChemCatChem* **2020**, *12*, 4387−4395.
(37) Wang, M.; Kang, J.; Xiong, X.; Zhang, F.; Cheng, K.; Zhang, Q.; Wang, Y. Effect of zeolite topology on the hydrocarbon distribution over bifunctional ZnAlO/SAPO catalysts in syngas conversion. *Catal. Today* **2020**, *371*, 85−92.
(38) Zhou, W.; Kang, J.; Cheng, K.; He, S.; Shi, J.; Zhou, C.; Zhang, Q.; Chen, J.; Peng, L.; Chen, M.; Wang, Y. Direct Conversion of Syngas into Methyl Acetate, Ethanol, and Ethylene by Relay Catalysis via the Intermediate Dimethyl Ether. *Angew. Chem., Int. Ed.* **2018**, *57*, 12012−12016.
(39) Jiao, W.; Su, J.; Zhou, H.; Liu, S.; Liu, C.; Zhang, L.; Wang, Y.; Yang, W. Dual template synthesis of SAPO-18/34 zeolite intergrowths and their performances in direct conversion of syngas to olefins. *Microporous Mesoporous Mater.* **2020**, *306*, 110444.
(40) Li, G.; Jiao, F.; Miao, D.; Wang, Y.; Pan, X.; Yokoi, T.; Meng, X.; Xiao, F.-S.; Parvulescu, A.-N.; Müller, U.; Bao, X. Selective conversion of syngas to propane over ZnCrO -SSZ-39 OX-ZEO catalysts. *J. Energy Chem.* **2019**, *36*, 141−147.
(41) Li, G.; Jiao, F.; Pan, X.; Li, N.; Miao, D.; Li, L.; Bao, X. Role of SAPO-18 Acidity in Direct Syngas Conversion to Light Olefins. *ACS Catal.* **2020**, *10*, 12370−12375.
(42) Yang, J.; Pan, X.; Jiao, F.; Li, J.; Bao, X. Direct conversion of syngas to aromatics. *Chem. Commun.* **2017**, *53*, 11146−11149.
(43) Ma, S.; Huang, S.-D.; Liu, Z.-P. Dynamic coordination of cations and catalytic selectivity on zinc-chromium oxide alloys during syngas conversion. *Nat. Catal.* **2019**, *2*, 671−677.
(44) Olsbye, U.; Svelle, S.; Bjørgen, M.; Beato, P.; Janssens, T. V. W.; Joensen, F.; Bordiga, S.; Lillerud, K. P. Conversion of Methanol to Hydrocarbons: How Zeolite Cavity and Pore Size Controls Product Selectivity. *Angew. Chem., Int. Ed.* **2012**, *51*, 5810−5831.
(45) Cheng, K.; Gu, B.; Liu, X.; Kang, J.; Zhang, Q.; Wang, Y. Direct and Highly Selective Conversion of Synthesis Gas into Lower Olefins: Design of a Bifunctional Catalyst Combining Methanol Synthesis and Carbon-Carbon Coupling. *Angew. Chem., Int. Ed.* **2016**, *55*, 4725−4728.
(46) Fu, Y.; Ni, Y.; Zhu, W.; Liu, Z. Enhancing syngas-to-aromatics performance of ZnO&H-ZSM-5 composite catalyst via Mn modulation. *J. Catal.* **2020**, *383*, 97−102.
(47) Liu, C.; Su, J.; Liu, S.; Zhou, H.; Yuan, X.; Ye, Y.; Wang, Y.; Jiao, W.; Zhang, L.; Lu, Y.; Wang, Y.; He, H.; Xie, Z. Insights into the Key Factor of Zeolite Morphology on the Selective Conversion of Syngas to Light Aromatics over a Cr2O3/ZSM-5 Catalyst. *ACS Catal.* **2020**, *10*, 15227−15237.
(48) Xu, Y.; Liu, J.; Wang, J.; Ma, G.; Lin, J.; Yang, Y.; Li, Y.; Zhang, C.; Ding, M. Selective Conversion of Syngas to Aromatics over Fe3O4@MnO2 and Hollow HZSM-5 Bifunctional Catalysts. *ACS Catal.* **2019**, *9*, 5147−5156.
(49) Miao, D.; Ding, Y.; Yu, T.; Li, J.; Pan, X.; Bao, X. Selective Synthesis of Benzene, Toluene, and Xylenes from Syngas. *ACS Catal.* **2020**, *10*, 7389−7397.
(50) Makeeva, D. A.; Kulikov, L. A.; Afokin, M. I.; Knyazeva, M. I.; Karakhanov, E. A.; Maksimov, A. L. Production of Aromatic Hydrocarbons from Syngas: Principles, Problems, and Prospects. *Russ. J. Appl. Chem.* **2020**, *93*, 933−953.
(51) Li, M.; Nawaz, M. A.; Song, G.; Zaman, W. Q.; Liu, D. Influential Role of Elemental Migration in a Composite Iron-Zeolite Catalyst for the Synthesis of Aromatics from Syngas. *Ind. Eng. Chem. Res.* **2020**, *59*, 9043−9054.
(52) Huang, Z.; Wang, S.; Qin, F.; Huang, L.; Yue, Y.; Hua, W.; Qiao, M.; He, H.; Shen, W.; Xu, H. Ceria-Zirconia/Zeolite Bifunctional Catalyst for Highly Selective Conversion of Syngas into Aromatics. *ChemCatChem* **2018**, *10*, 4519−4524.
(53) Cheng, K.; Zhou, W.; Kang, J.; He, S.; Shi, S.; Zhang, Q.; Pan, Y.; Wen, W.; Wang, Y. Bifunctional Catalysts for One-Step Conversion of Syngas into Aromatics with Excellent Selectivity and Stability. *Chem* **2017**, *3*, 334−347.
(54) Song, H.; Laudenschleger, D.; Carey, J. J.; Ruland, H.; Nolan, M.; Muhler, M. Spinel-Structured ZnCr2O4 with Excess Zn Is the Active ZnO/Cr2O3 Catalyst for High-Temperature Methanol Synthesis. *ACS Catal.* **2017**, *7*, 7610−7622.
(55) Liu, J.; He, Y.; Yan, L.; Li, K.; Zhang, C.; Xiang, H.; Wen, X.; Li, Y. Nano-sized ZrO2 derived from metal-organic frameworks and their catalytic performance for aromatic synthesis from syngas. *Catal. Sci. Technol.* **2019**, *9*, 2982−2992.
(56) Raveendra, G.; Li, C.; Cheng, Y.; Meng, F.; Li, Z. Direct transformation of syngas to lower olefins synthesis over hybrid Zn-Al2O3/SAPO-34 catalysts. *New J. Chem.* **2018**, *42*, 4419−4431.
(57) Santos, V. P.; Pollefeyt, G.; Yancey, D. F.; Ciftci Sandikci, A.; Vanchura, B.; Nieskens, D. L.; de Kok-Kleiberg, M.; Kirilin, A.; Chojecki, A.; Malek, A. Direct conversion of syngas to light olefins (C2-C3) over a tandem catalyst CrZn-SAPO-34: Tailoring activity

https://doi.org/10.1021/acsomega.2c05225
ACS Omega 2022, 7, 42994−43005

and stability by varying the Cr/Zn ratio and calcination temperature. *J. Catal.* **2020**, *381*, 108−120.
(58) Yang, X.; Su, X.; Liang, B.; Zhang, Y.; Duan, H.; Ma, J.; Huang, Y.; Zhang, T. The influence of alkali-treated zeolite on the oxide-zeolite syngas conversion process. *Catal. Sci. Technol.* **2018**, *8*, 4338−4348.
(59) Zhou, H.; Liu, S.; Su, J.; Liu, C.; Zhang, L.; Jiao, W.; Wang, Y. Light Olefin Synthesis from Syngas over Sulfide-Zeolite Composite Catalyst. *Ind. Eng. Chem. Res.* **2018**, *57*, 6815−6820.
(60) Lai, Z.; Sun, N.; Jin, J.; Chen, J.; Wang, H.; Hu, P. Resolving the Intricate Mechanism and Selectivity of Syngas Conversion on Reduced ZnCr2Ox: A Quantitative Study from DFT and Micro-kinetic Simulations. *ACS Catal.* **2021**, *11*, 12977−12988.
(61) Wang, C.-M.; Wang, Y.-D.; Xie, Z.-K. Methylation of olefins with ketene in zeotypes and its implications for the direct conversion of syngas to light olefins: a periodic DFT study. *Catal. Sci. Technol.* **2016**, *6*, 6644−6649.

https://doi.org/10.1021/acsomega.2c05225
ACS Omega 2022, 7, 42994−43005